J. Iron Steel Res. Int.
https://doi.org/10.1007/s42243-024-01347-7

ORIGINAL PAPER

In-situ observation and analysis of high temperature behavior of carbides in GCr15 bearing steel by confocal laser scanning microscopy

Jun Ren[1,2] · Yue Teng[1,2] · Xiang Liu[3] · Xi Xu[3] · Hui-gai Li[1,2] · Ke Han[4] · Qi-jie Zhai[2]

Received: 28 February 2024 / Revised: 28 April 2024 / Accepted: 28 May 2024
© China Iron and Steel Research Institute Group Co., Ltd. 2024

Abstract
The high-temperature dissolution behavior of primary carbides in samples taken from GCr15 continuous-casting bloom was observed in-situ by confocal laser scanning microscopy. Equations were fitted to the dissolution kinetics of primary carbides during either heating or soaking. Dissolution of carbides proceeded in three stages (fast → slow → faster) as either temperature or holding time was increased. During the heating process and during the first and third stages of the soaking process, the original size of the carbides determined the steepness of the slope, but during the middle ("slow") stage of the soaking process, the slope remained zero. The initial size of the carbides varied greatly, but their final dissolution temperature fell within the narrow range of 1210–1235 °C, and the holding time remained within 50 min. Fractal analysis was used to study the morphological characteristics of small and medium-sized carbides during the dissolution process. According to changes in the fractal dimension before and after soaking, the carbides tended to evolve towards a more regular morphology.

Keywords Bearing steel · High-temperature confocal laser scanning microscope · In-situ observation · Primary carbide · Fractal analysis

1 Introduction

Carbides strengthens GCr15 bearing steel [1–5]. Fine and evenly distributed primary carbides can provide good wear resistance and significantly improve the rotational bending fatigue strength and rolling contact fatigue life of GCr15 bearing steel [6]. Low impact toughness of GCr15 bearing steel has been related to the low density of carbides [7]. During the solidification process of liquid steel, Cr and C elements are enriched in the dendrites, resulting in segregation at the end of solidification [8–10].

Segregation easily leads to the formation of large primary carbides. The type of primary carbide in GCr15 steel is mainly chromium-containing cementite $(Fe, Cr)_3C$ [11]. Coarse carbides are detrimental to the service life of the bearings [12]. Fukaura et al. [13] found that the refinement of primary carbide can enhance the fatigue properties. The study of Yang et al. [14] indicated that the equivalent diameter of the primary carbide can be controlled at 5–10 μm to achieve the best tribological properties. In order to refine carbides, Zhou et al. [15] promoted the nucleation of carbides during solidification by adding rare earth elements. In addition, Kim and Bae [16] found that adding rare earth elements in bearing steel can reduce the segregation of alloying elements and reduce the size of primary carbides. Du et al. [17] studied the precipitation process of carbides in GCr15 steel during solidification and found that the size of primary carbides decreased significantly with

✉ Hui-gai Li
lihuigai@shu.edu.cn

1 State Key Laboratory of Advanced Special Steel and Shanghai Key Laboratory of Advanced Ferrometallurgy and School of Materials Science and Engineering, Shanghai University, Shanghai 200444, China

2 Center for Advanced Solidification Technology (CAST), School of Materials Science and Engineering, Shanghai University, Shanghai 200444, China

3 Ansteel Group Iron and Steel Research Institute, Anshan 114000, Liaoning, China

4 National High Magnetic Field Laboratory, Florida State University, Tallahassee, FL 32310, USA

Published online: 10 October 2024

the increase in cooling intensity. To refine various carbides in steels by either addition of alloying elements or engineering the process parameters, researchers have been trying to study the carbide formation using various ex situ microscopy techniques [18–20]. However, it is desirable to examine the formation in situ. Researchers started to use confocal laser scanning microscope (CLSM), which had been developed recently, to study in situ carbide formations. Using CLSM, the evolution of carbides in steel can be dynamically observed at high temperature. Different from traditional methods [21–23], this method can examine the changes of morphology and size at high temperatures [24–26]. For example, researchers have examined the effect of cooling rate on carbide precipitation and showed that when the cooling rate is greater than 300 K/min, the average diameter of the carbides is below 7 μm, accompanied by an increase in the number of carbides.

At present, there are few in-situ studies on the evolution of carbides at high temperature in GCr15 steel. This paper reports our studies of the dissolution characteristics of carbides in GCr15 steel during heating through CLSM, which on the one hand helps to understand the dissolution behavior of carbides in this steel at high temperature and on the other hand provides reference for the formulation of relevant heat treatment processes.

2 Experimental materials and methods

Five ϕ8 mm × 3.5 mm samples (S1, S2, S3, S4, and S5) were taken near the center of the cross section of a 280 mm × 380 mm GCr15 continuous casting bloom. We found that massive carbides (> 30 μm in size) tended to exist at the central portion of the cross section of blooms [25]. The chemical composition of the samples is shown in Table 1. To expose carbides, samples were sanded and polished, and then etched with 4 vol.% Nital solution. Primary carbides of different sizes were selected for in-situ CLSM observation. The CLSM model was LasertecTMVL2000DX-SVF17SP. In the argon atmosphere, the magnification of the microscope was set to 550×, and the in-situ observation experiment was carried out. S1 to S4 were for the observation of original large-size primary carbide dissolution process, and S5 was for the observation of the partly-dissolved small-size carbide dissolution process.

Okamoto et al. [27] gave the formula for massive carbide (tens of microns) dissolution by the diffusion soaking of bearing steel:

$$\ln t_h \approx 86{,}300/T_h - 44.56 + \ln\left(2.5a_C^2/4\right) \quad (1)$$

where t_h is the dissolution time of massive carbide, h; T_h is the holding temperature of homogenization heat treatment, °C; and a_C is the diameter of massive carbide, cm.

According to Eq. (1), carbide is approximately regarded as a circle, the dissolution curve of carbides in bearing steel at 1190–1250 °C was obtained (Fig. 1), and the carbides with an area of about 1300 μm^2 can be completely dissolved at 1230 °C for 1 h. Accordingly, the parameters for carbide dissolution in S1–S4 were set at 1230 °C for 60 min as shown in Fig. 2. The dissolution difference of different sizes was observed. Because of the lower heating rate set for S1–S4, the carbides dissolved completely after the beginning of soaking. To learn the dissolution dynamics of carbides during soaking process, we needed to avoid the thorough dissolution of carbides before soaking, so we increased the heating rate, slightly reduced the holding temperature (1220 °C), and shortened the holding time (30 min) for S5. The cooling rate was set at 300 °C/min.

The dissolution behavior of carbides with increasing temperature or time was in-situ observed, and the size evolution of carbides was obtained. The conditions of each sample are listed in Table 2.

The entire process of carbide dissolution was recorded by a video recorder of the CLSM. The size of carbides in the video screenshot recorded in the experiment was measured by ImageJ. The morphologies and distributions of carbides in five samples before and after the experiments were observed under a field emission scanning electron microscope (SEM) JSM-IT800. The original large-size carbides during heating were measured by area because of their large length to width ratio, and 30 measured values were obtained from images captured every 15–20 °C. The dissolved small-size carbides during holding were measured by diameter, and 12 measured values were obtained from images captured every 2.5 min.

Fractal analysis [28] was used to calculate the fractal dimension of carbide morphology before and after soaking to study the morphology and size change of the carbides. Binary processing was carried out on the metallographic photos obtained by in-situ experiment. The boundary

Table 1 Chemical composition of test steel (wt.%)

Element	C	Si	Mn	Cr	P	S	Ni	Al	Ti
Content	0.98	0.28	0.30	1.48	≤ 0.015	≤ 0.008	≤ 0.15	≤ 0.03	≤ 0.003

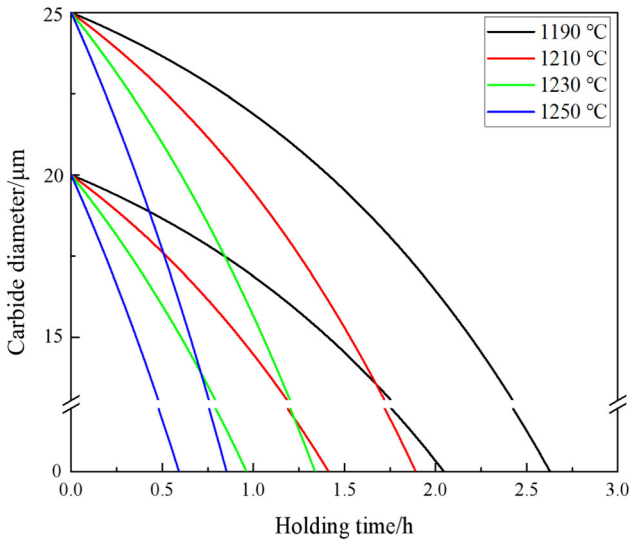

Fig. 1 Dissolution curve of carbide in bearing steel

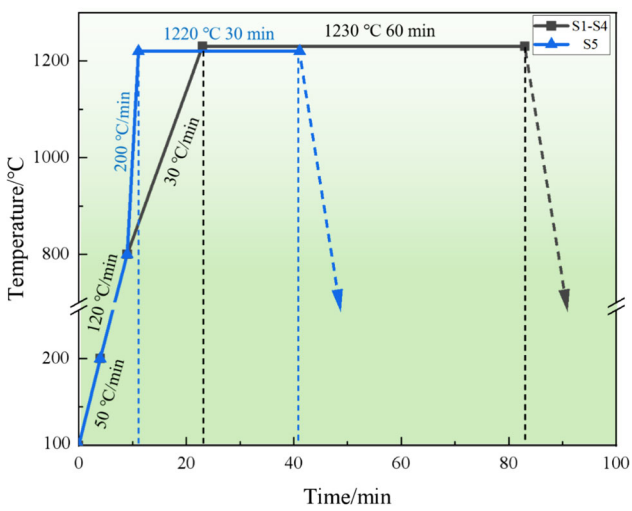

Fig. 2 High-temperature laser confocal parameter setting

contour of the binary image was drawn (Fig. 3). We covered all the contour curves of all the rough fractal surfaces with several square boxes with the side length δ and recorded the empty intersection between the box and the image as 0 and the non-empty intersection as 1. We calculated the number of all the boxes with 1 and recorded it as $N(\delta)$, so that a group of $(\delta, N(\delta))$ was obtained. Then, we reduced the side length of the box. When δ approached 0, $N(\delta)$ gradually tended to positive infinity, and a series of $(\delta, N(\delta))$ were obtained by taking $\ln\delta$ as the horizontal coordinate and $\ln N(\delta)$ as the vertical coordinate. A function graph was plotted, and the slope was calculated. The slope is the fractal dimension of the image.

3 Results and discussion

3.1 Influence of temperature on carbide dissolution

In samples S1 to S4, the changes in carbide area that resulted from changes in temperature were statistically analyzed in order to deduce the kinetic relationship between temperature and carbide dissolution (Fig. 4). The dissolution laws of carbides of different sizes are similar. The difference is that the smaller the original size of the carbide, the earlier the transition temperature at each stage.

The linear fitting curves of the area (S) of four different original sizes of carbides versus heating temperature were obtained at each stage. Therefore, expressing the slope and intercept in terms of the original area gave a uniform equation. The fitting formula was shown in Table 3. In each stage, the slope of the formula depended on the original size, and the steepness of the slope decreased with the decrease in the original size. The results showed that even though the initial size of the primary carbides varied greatly, the final dissolution temperature of these carbides fell within a small range of 1210–1235 °C.

We divided the dissolution of carbides during heating process into three stages: (1) initial—relatively rapid dissolution stage; (2) middle—slow dissolution stage; and (3) final—rapid dissolution stage. In the initial stage, chemical potential is the driving force for the dissolution of carbides. This occurs because of a large difference between carbide

Table 2 Annealing conditions of S1–S5

No.	Original carbide area/ μm^2	Original carbide equivalent diameter/ μm	Heating rate/(°C min^{-1})	Holding temperature/ °C	Holding time/ min
S1	1436	43	30	1230	60
S2	1351	41	30	1230	60
S3	1207	39	30	1230	60
S4	532	26	30	1230	60
S5	1398	42[1)]	200	1220	30

[1)]42 μm refers to length of original carbide in S5, which became 24 μm when temperature rose to 1220 °C and soaking began

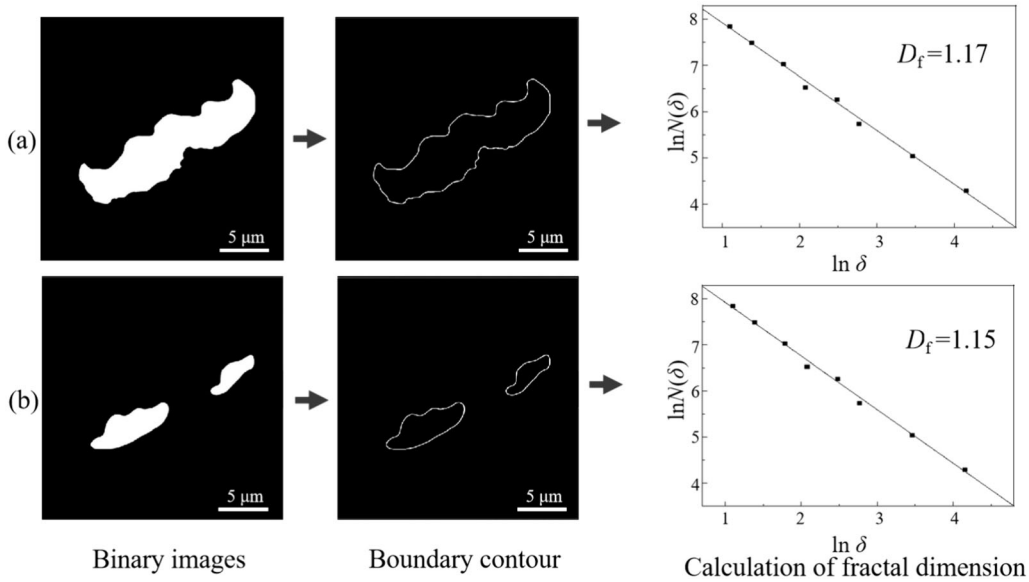

Fig. 3 Fractal dimension calculation process. **a** Before holding; **b** after holding (take strip carbide 3 as an example). D_f is fractal dimension, measuring morphological complexity of object δ and $N(\delta)$, and is a dimensionless parameter

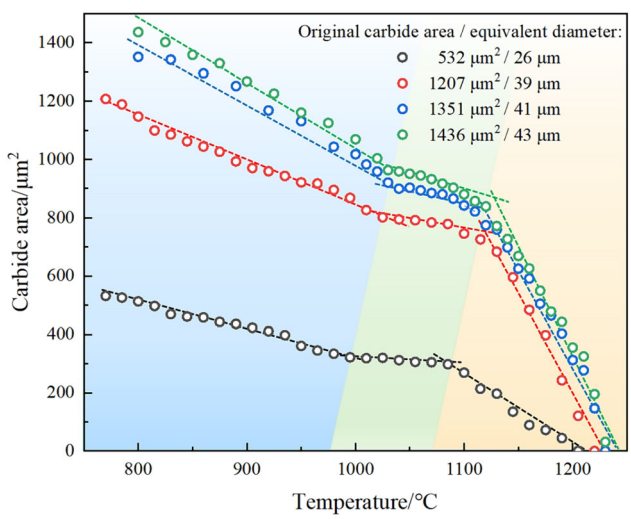

Fig. 4 Area changes of carbides during heating. Blue area represents initial stage—relatively rapid dissolution; green area represents middle stage—slow dissolution; and yellow area represents final stage—rapid dissolution

and matrix with respect to the composition of carbon, against the background of modest temperature and low element diffusion coefficient. The chemical potential of carbon remained constant in the carbide and in the bearing steel matrix that was relatively distant from the interface. The chemical potential gradually increased, however, in the bearing steel matrix that was nearer to the interface (Fig. 5a). The chemical potential of C increases with increasing temperature [29], but that of the difference between the carbide and the interface decreases (Fig. 5a). At temperature T_1, the chemical potential difference of C between carbide and nearby matrix (interface) was μ_{ab}. As the temperature increased, the chemical potential difference decreased gradually, and when the temperature rose to T_2, the chemical potential difference of C between the carbide and the nearby matrix (interface) was μ_{cd}. It was reported that the chemical potential difference between two phases decreases at elevated temperature [30]. When the temperature rose to T_3 (about 975–1050 °C in Fig. 4), the chemical potential difference of C between the carbide and the nearby matrix disappeared (point e in Fig. 5a). This resulted in the slowing down of the dissolution rate of the carbides.

As temperature increases, the element diffusion coefficient increases. Diffusion becomes the dominant factor that affects the dissolution process of carbide. The diffusion coefficient D is expressed as Eq. (2) [31]:

$$D = D_0 \exp^{-Q/(RT)} \tag{2}$$

where D_0 is the diffusion constant; Q is the diffusion activation energy, kJ/mol; R is the gas constant (8.314 J/(mol K)); and T is the absolute temperature, K.

According to our calculated diffusion coefficients for C and Cr in GCr15 steel, the diffusion coefficient of these elements increased as temperature increases. When the holding temperature increased from about 1100 to 1230 °C, the diffusion coefficient of C and Cr was nearly doubled (Fig. 5b), which led to an increase in the carbide dissolution rate.

All carbides began to transform into spheroids after the temperature reached 1125 °C. By 1200 °C, most of the carbides had become spheroids. Dispersion of fine primary carbides can effectively increase wear resistance and

Table 3 Fitting results of primary carbide dissolution kinetics with temperature change

Initial (R^2 = 0.91)	Middle (R^2 = 0.94)	Final (R^2 = 0.86)	Remark
$S_1 = a - bT$	$S_2 = c - dT$	$S_3 = m - nT$	$a = 2S_0 + 66$
			$b = 0.0012S_0 + 0.16$
			$c = \exp\left(6 - 2 \times 10^{-4}S_0 + 9 \times 10^{-7}S_0^2\right)$
			$d = 0.002 \times \exp(0.0044S_0) + 0.24$
			$m = -30{,}832 \times \exp(-0.0032S_0) + 8703$
			$n = -38 \times \exp(-0.0041S_0) + 6.8$

R^2 is fitting correlation coefficient (The closer the R^2 is to 1, the better the fit); parameters a, b, c, d, m, and n are related to original area of carbide S_0; and T is calculated in °C

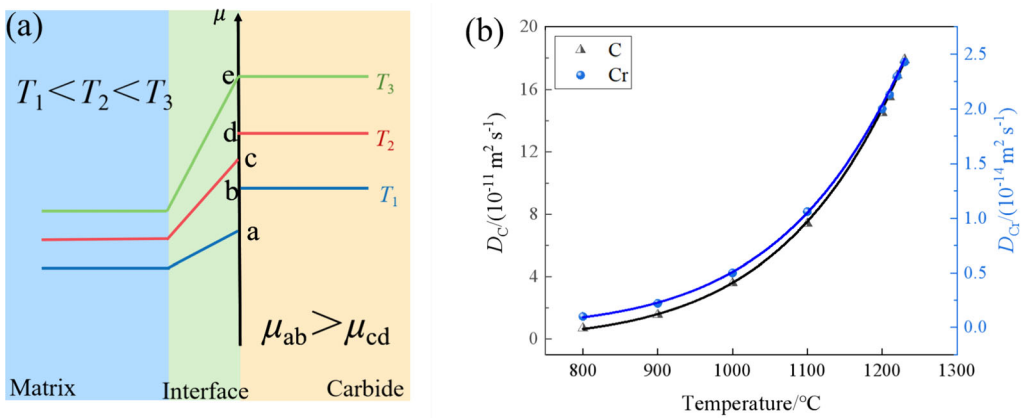

Fig. 5 Schematic diagram of changes of chemical potential of C at different temperatures (**a**) and diffusion coefficients of C and Cr (**b**)

fatigue life in GCr15 steel by reducing the formation of cracks during quenching [32]. To obtain fine-sphere carbides, we recommend that thermal soaking temperature be set at 1200 °C. To get complete dissolution of primary carbides, however, it would be better to set thermal soaking temperature in the range of 1210–1235 °C.

3.2 Disconnection and spheroidization of primary carbides

As shown in Fig. 6, carbides appear as white blocks in the field center. Notches form on weak areas wherever the carbide boundary is not straight. Between 725 and 825 °C, the size and the isthmus-like morphology of carbides (including the sizes and shapes of notches) remained unchanged. Between 925 and 1025 °C, the larger carbides began to narrow. Between 1025 and 1125 °C, the narrower carbides began to separate at the notches into smaller, lumpier, and island-like shapes. These island-like carbides became more spherical as the temperature increased above 1125 °C, and the carbides break from notches. By about 1200 °C, all the carbides had become clearly spheroidic (Fig. 6). The morphology and element distribution of the carbide before and after heating obtained by SEM could also confirm that the carbide had been completely dissolved (Fig. 7).

Because curvature at the notch is small, interfacial energy is higher there. The notch region should dissolve preferentially to transform into a stable and low-energy state [33, 34]. During the heating process, the alloying elements in the carbide tended to spread outward from these smaller notches to places with larger curvature radii (i.e., to larger notches or even to the flat surface of the carbide itself). We found that carbides were preferentially dissolved within the notches. When this happened, the dissolving carbides changed the radii of the notches, thus destroying the balance of interfacial tension. This state of disequilibrium caused the carbides to continue to dissolve until each carbide divided into at least two parts, usually disconnecting from each other at sharp corners and necking positions.

As the temperature continued to rise, the carbides continued to dissolve and their volume fraction continued to decrease. In the third stage, the dissolution rate changed from slow to fast. We attribute this increased rate to increased interface energy resulting from the spheroidization process (Fig. 8). Once the temperature reached 1125 °C, all the carbide had been broken down from a few

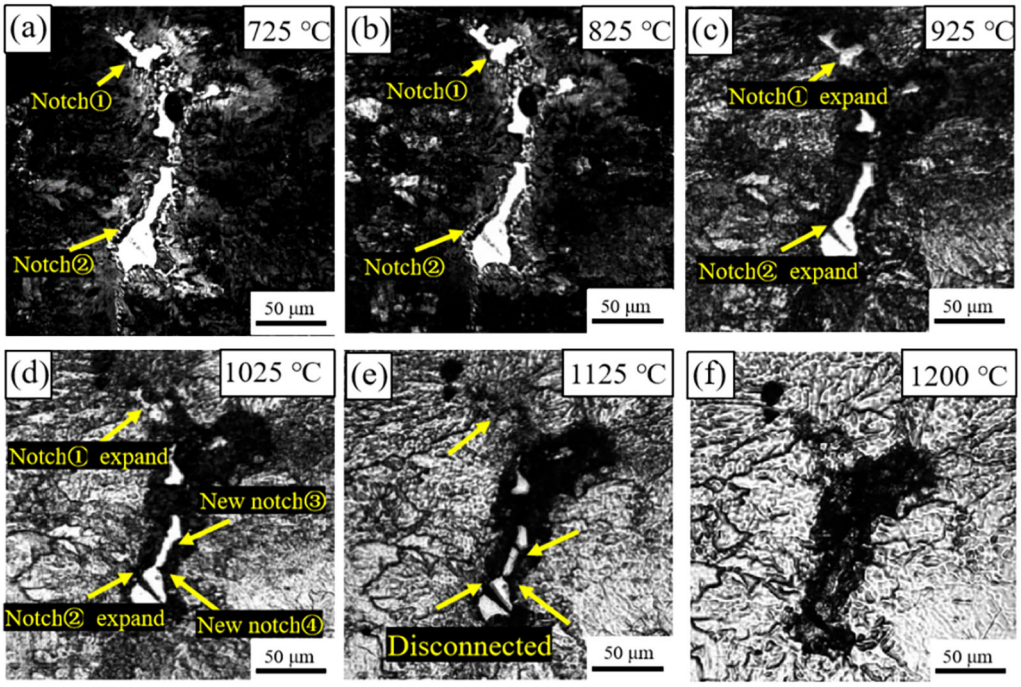

Fig. 6 In-situ observation of carbides in S1 during heating process

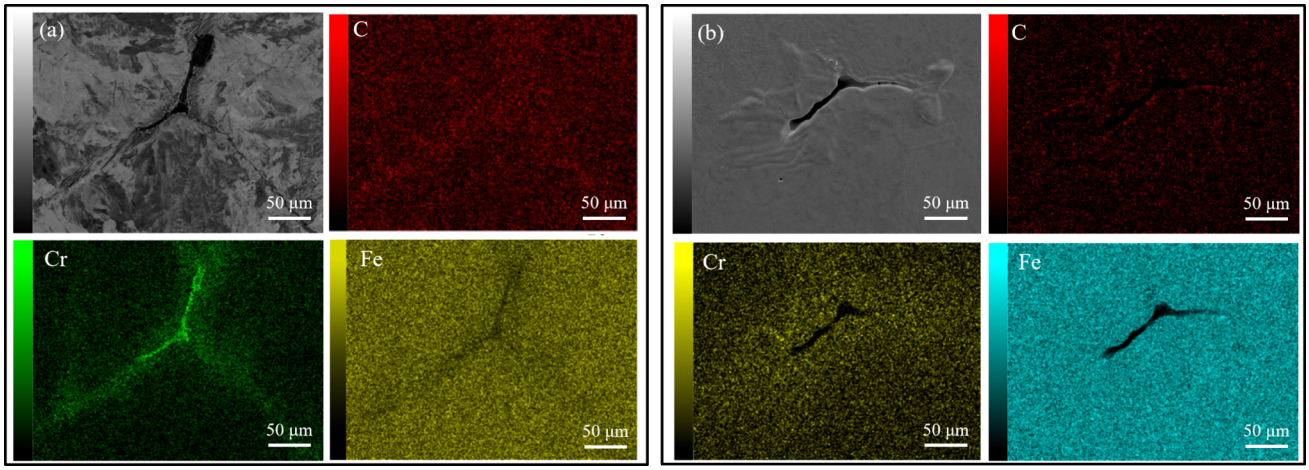

Fig. 7 Second electron image of a carbide and its map scanning showing element distribution. **a** Before heating; **b** after heating

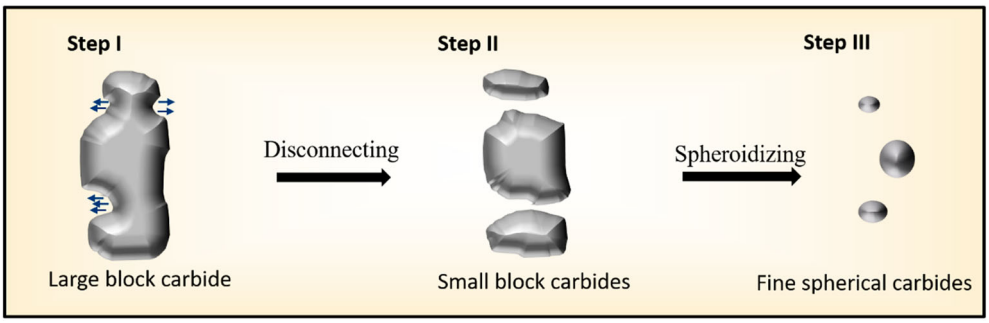

Fig. 8 Schematic diagram showing breaking and spheroidizing of carbides

large blocks into many small blocks. By that point, the corners of the small block carbides had small radii and thus became the preferential dissolution region, as the result of the Gibbs–Thomson effect [35]. It was this dissolution that led to the formation of spherical carbides. Under high temperature conditions, carbides are continuously dissolved under the influence of curvature, the edges tend to be rounded, and the carbides turn into spherical distributions [36]. This promotes the dissolution of the carbide.

3.3 Influence of holding time on carbide dissolution

The dissolution of carbides in S5 during the holding process was observed in-situ. The average size of the carbides in S5 was smaller than 24 μm. Before soaking at 1220 °C, the morphology of the carbides has been long and either nearly round or irregular in shape. During the 30 min soaking, almost all of the carbides gradually decreased in size and changed to consistently round shapes. Comparison of the binary images of carbides before and after soaking shows the reduction in the complexity of the carbide shapes (Fig. 9).

The fractal dimension of carbides was 1.15–1.23 before soaking and 1.14–1.17 afterward. After soaking, the carbides became more regular in shape; i.e., the values of the fractal dimension associated with different morphologies all decreased after soaking. From the difference in fractal dimension before and after soaking, it can be seen that the larger the fractal dimension of carbide before soaking (that is, the greater the complexity), the greater the reduction in the fractal dimension after soaking, indicating that carbides with more complex morphology tended to develop in the direction of simpler, more regular shapes (Fig. 10).

The statistical size changes of carbides with respect to different holding time were fitted by linear regression (Fig. 11). The dissolution rate changed from fast to slow due to the influence of concentration gradient in the early stage. In the later stage, the morphology of carbides tended to be regular, which promoted the dissolution rate of carbides. The blue area in Fig. 11 was the initial stage, in which the carbide dissolved relatively quickly; the green area was the middle stage of dissolution, which dissolved

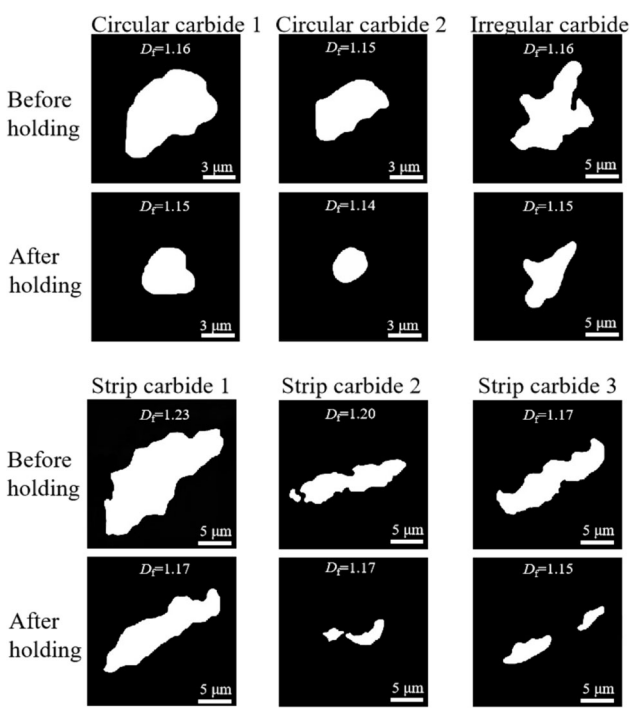

Fig. 9 Morphology of carbides

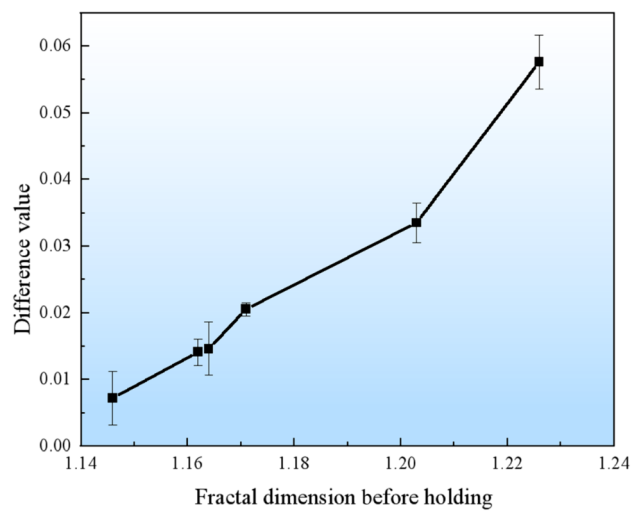

Fig. 10 Difference in fractal dimension before and after soaking

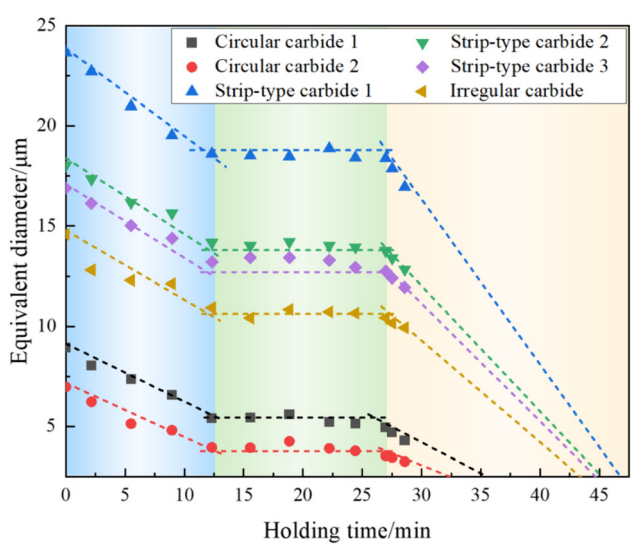

Fig. 11 Changes of carbide size with holding time

Table 4 Fitting results of carbide dissolution kinetics with holding time

$0 \le t < 12$ (R^2 = 0.90)	$12 \le t < 27$ (R^2 = 0.85)	$t \ge 27$ (R^2 = 0.87)	Remark
$d_1 = A - Bt$	$d_2 = 0.9d_0 - 2.5$	$d_3 = 1.85A - Ct - 2.87$	$A = d_0 + 0.2$ $B = 0.01d_0 + 0.2$ $C = 0.035d_0 - 0.004$

A, B, and C are parameters related to original size of carbide d_0; and t is holding time, min

slowly and was represented as a platform area; the yellow area was the last stage of dissolution with rapid dissolution rate. When the holding time $t < 12$ min and $t \ge 27$ min, the carbide size was related to both the holding time and the original size. When the holding time was between 12 and 27 min, the carbide size was related only to the original size (Table 4). The size range of the carbides applicable to the equation was 5–25 μm. All carbides could be dissolved within 50 min of soaking (see Fig. 11).

Combining the fitting results of Sects. 3.1 and 3.3, we concluded that the changes in massive carbides that occurred with the increase in temperature were very similar to changes that occurred with the increase in holding time, showing a fast → slow → faster trend. With respect to the dissolution of carbides during soaking, the effect of the initial carbide diameter was larger than that of the holding time. In the early stage, the dissolution rate of carbides was also affected by the concentration gradient. Due to the high concentration gradient in the vicinity of the interface between the carbides and the matrix, the dissolution rate of carbides was relatively fast. With each extension of holding time, the concentration gradient decreased, resulting in a gradual decrease in the dissolution rate, which came to resemble a plateau (see Fig. 11). When the holding time was further extended, the morphology of the carbides gradually became regular, and the number of the carbides increased, which resulted in the increased interface area (for strip-type carbide 3, the areas before and after breaking were 0.8 and 1.2 $\mu m^2/\mu m^3$), and then, the carbide dissolution rate increased.

4 Conclusions

1. The dissolution of primary carbides during heating or soaking proceeded rapidly at first, then slowly, and then even more rapidly. The final dissolution temperature of the carbides was in the narrow range of 1210–1235 °C. Carbides with more complex morphology tended to develop in the direction of simpler, more regular shapes during soaking. All carbides could be dissolved within 50 min of soaking.
2. The dissolution kinetics of primary carbides during heating was quantified by fitting linear functions to carbide area as temperature increased. The coefficients of the functions were related to the original area. These coefficients had a linear relationship with S_0 in the initial stage, a second-order exponential relationship in the middle stage, and an exponential relationship in the final stage.
3. The kinetics of carbide dissolution during the soaking process were established. For holding time of $t < 12$ min and $t \ge 27$ min, the indicated carbide size was related to both the original carbide size and the holding time. Carbide size and holding time had a linear relationship, and the coefficients of the functions were related to the original carbide size. When t was between 12 and 27 min, carbide size exhibited a linear relationship solely with the original size, irrespective of the holding time.

Acknowledgements This work was supported by Independent Research Project of State Key Laboratory of Advanced Special Steel, Shanghai Key Laboratory of Advanced Ferrometallurgy, Shanghai University (SKLASS-2023-Z13) and the Science and Technology Commission of Shanghai Municipality (No. 19DZ2270200). A portion of the work was performed at US National High Magnetic Field Laboratory, which is supported by the National Science Foundation (Cooperative Agreement No. DMR-1157490 and DMR-1644779) and the State of Florida. Thanks also to Mary Tyler for editing.

Declarations

Conflict of interest Qi-jie Zhai is an editorial board member for *Journal of Iron and Steel Research International* and was not involved in the editorial review or the decision to publish this article. All authors certify that they have no affiliations with or involvement in any organization or entity with any financial interest or non-financial interest in the subject matter or materials discussed in this manuscript.

References

[1] X. Wang, G. Li, Y. Liu, Y. Cao, F. Wang, Q. Wang, Metals 9 (2019) 1247.
[2] H.Y. Zhao, Metall. Mater. 41 (2021) 185–186.
[3] C.J. Li, W.M. Li, J. Iron Steel Res. Int. 29 (2022) 1899–1900.
[4] A. Kootsookos, J.D. Gates, Mater. Sci. Eng. A 490 (2008) 313–318.
[5] G.H. Zhu, G. Zheng, Front. Mater. Sci. China 2 (2008) 72–75.
[6] Z. Cao, Z. Shi, F. Yu, K.I. Sugimoto, W. Cao, Y. Weng, Int. J. Fatigue 128 (2019) 105176.

[7] Y.H. Kong, S.B. Li, J.L. Zhou, S.G. Zhu, Heat Treat. Met. 41 (2016) 95–99.
[8] M. Wang, X. Zha, M. Gao, Y. Ma, K. Liu, Y. Li, Metall. Mater. Trans. A 46 (2015) 5217–5231.
[9] Y. Tian, M.C. Zhao, Y.P. Zeng, X.B. Shi, W. Yan, K. Yang, T.Y. Zeng, JOM 74 (2022) 2409–2419.
[10] N. Zong, S. Ma, W. Sun, T. Jing, Z. Lu, Metall. Ital. 11 (2020) 14–22.
[11] D. Jiang, L. Zhang, Steel Res. Int. 92 (2021) 458–463.
[12] S.S. Li, Y. Chen, T.Z. Gong, X.Q. Chen, P.X. Fu, D.Z. Li, Acta Metall. Sin. 58 (2022) 1024–1034.
[13] K. Fukaura, Y. Yokoyama, D. Yokoi, N. Tsujii, K. Ono, Metall. Mater. Trans. A 35 (2004) 1289–1300.
[14] Q. Yang, T. Senda, A. Ohmori, Wear 254 (2003) 23–34.
[15] X. Zhou, X. Yin, F. Fang, J. Jiang, W. Zhu, J. Rare Earths 30 (2012) 1075–1078.
[16] K.H. Kim, C.M. Bae, Met. Mater. Int. 19 (2013) 371–375.
[17] G. Du, J. Li, Z.B. Wang, Metall. Mater. Trans. B 48 (2017) 2873–2890.
[18] K. Han, T.D. Mottishaw, G.D.W. Smith, D.V. Edmonds, A.G. Stacey, Mater. Sci. Eng. A 190 (1995) 207–214.
[19] K. Han, G.D.W. Smith, D.V. Edmonds, Metall. Mater. Trans. A 26 (1995) 1617–1631.
[20] K. Han, T.D. Mottishaw, G.D.W. Smith, D.V. Edmonds, Mater. Sci. Tech. 10 (1994) 955–963.
[21] F. Han, L. Jiang, X. Ye, Y. Lu, Z. Li, X. Zhou, Materials 10 (2017) 521.
[22] X.F. Zhou, F. Fang, J.Q. Jiang, W.L. Zhu, H.X. Xu, Mater. Sci. Technol. 30 (2014) 116–122.
[23] J. Zhang, J. Li, C. Shi, J. Huang, J. Mater. Res. Technol. 11 (2021) 1490–1505.
[24] G.C. Gu, R. Pesci, L. Langlois, E. Becker, R. Bigot, M.X. Guo, Acta Mater. 66 (2014) 118–131.
[25] Q.T. Zhu, J. Li, C.B. Shi, W.T. Yu, C.M. Shi, J.H. Li, Int. J. Mater. Res. 108 (2017) 20–28.
[26] W.M. Li, S.C. Jiao, W.J. Tong, J. Iron Steel Res. Int. 28 (2020) 990–996.
[27] K. Okamoto, S. Shikō, T. Ōta, ISIJ Int. 7 (1967) 197–204.
[28] Z. Liu, F.B. Yu, The Chinese Journal of Nonferrous Metals 19 (2009) 228–234.
[29] J. Zhang, M.B. Clennell, D.N. Dewhurst, K. Liu, Fuel 122 (2014) 186–197.
[30] G.F. Mi, W.L. Gao, H.W. Wang, Y.X. Jin, Ti-based in-situ composite, China Mining University Press, Xuzhou, China, 2005.
[31] G.X. Hu, X. Cai, Y.H. Rong, Fundamentals of materials science, Shanghai Jiao Tong University Press, Shanghai, China, 2010.
[32] G.L. Hu, Heat treatment of steel, Northwestern Polytechnical University Press, Xi'an, China, 2010.
[33] W.M. Gui. X.T. Zhang, H.Y. Zhang, J. Alloy. Compd. 787 (2019) 152–157.
[34] Y.T. Wang, Y. Adachi, K. Nakajima, Y. Sugimoto, Acta Mater. 58 (2010) 4849–4858.
[35] M. Perez, Scripta Mater. 52 (2005) 709–712.
[36] Z.Q. Li, Z. Wen, F.Y. Su, Int. J. Mater. Res. 107 (2016) 372–380.

Springer Nature or its licensor (e.g. a society or other partner) holds exclusive rights to this article under a publishing agreement with the author(s) or other rightsholder(s); author self-archiving of the accepted manuscript version of this article is solely governed by the terms of such publishing agreement and applicable law.